2022

Modeling of Ice Harvest and Dispensing Processes of Domestic Icemaker Systems Using DEM

Elizabeth Wohlers

Lucilla Coelho de Almeida

Vinicius Daroz

Modeling of Ice Harvest and Dispensing Processes of Domestic Icemaker Systems using DEM

Elizabeth Wohlers[1*], Lucilla Coelho de Almeida[2], Vinicius Daroz[2]

[1] Sub-Zero Group, Inc.,
Madison, WI, USA
elizabeth.wohlers@subzero.com

[2] ESSS,
Florianópolis, SC, Brazil
lucilla@esss.co
vdaroz@esss.co

* Corresponding Author

ABSTRACT

Ice damage, poor ice sensing and displaced ice are common issues in the design of various types of ice dispensing systems found in domestic household refrigeration units. These issues are often not seen until the design has already been prototyped, which can lead to multiple design iterations, field issues and customer dissatisfaction. This study will address the feasibility of using discrete element modeling (DEM) techniques to simulate the harvest and dispensing processes of two types of domestic ice dispensing systems in order to optimize component design and system function. Custom polyhedral particles were used to model the actual crescent shape of the ice, increasing the accuracy of the model by properly capturing the ice-ice and ice-dispenser interactions. The complete collision statistics data set can provide useful information such as the stress distribution over the particle and boundary surfaces, allowing for ice damage prediction as well as impact intensities on the container that the ice is dispensed into. Additionally, the solution of the ice dispenser mechanism using a free body dynamics motion kernel can account for the ice build-up inside the bucket under the ice maker control arm and is capable of predicting whether the selected design is efficient in preventing ice particles from falling off the back of the bucket during customer usage. The developed models can be used as a design tool, giving directions on how to improve the existing models and reducing the number and cost of prototype cycles.

1. INTRODUCTION

Iterative prototyping design methods for consumer ice dispensing systems have been commonplace in industry due to the lack of readily available modeling tools that accurately predict the behavior of ice during harvest and dispensing. Traditional simulation methods like Computational Fluid Dynamics (CFD) cannot predict how individual particles will behave and early DEM codes have required the simplification of particle shape into either a sphere or the glued spheres method, which significantly degrades the accuracy of the results if actual particles have sharp edges. Newer DEM codes are now able to use actual particle shapes for more accurate contact detection and are also capable of modeling adhesion and breakage as well as providing an array of post processing features that allow for the study of impact forces, residence time, and visualization of particle flow. For this reason, DEM has been gaining traction as a cost effective, time-saving design tool for dispensing processes in food production, pharmaceutical, agriculture and mining industries and therefore also lends itself well to the consumer appliance industry. There are a number of studies using DEM to evaluate similar types of dispensing systems. Fernandez et al. (2009) discuss how different screw feeder designs affect the mixing and dispensing rates of spherical particles in a hopper dispensing system. There are also a small but growing number of studies looking at non-spherical particles in dispensing systems. Sun et al. (2022) discuss the interaction of particle shape and screw blade design in an auger dispensing system with regards to mass flow, contact forces and particle damage. This study builds upon existing research to discuss the modeling of a uniquely shaped ice particle which is used to characterize the harvest cycle and two types of ice dispensing methods.

2. OVERVIEW OF ICEMAKER HARVEST AND DISPENSING SYSTEMS

2.1 Harvest Operation

The icemaker in this study operates by first calling for a prescribed amount of water to be dispensed into the ice mold from the inlet cup (100–110 mL). The mold consists of 8 crescent shaped cavities with a channel running parallel to the length of the mold, which allows water to fill all cavities, as shown in Figure 1a. The ice is allowed to freeze until the built-in thermostat reaches −9.44 °C. Next, a heater under the mold turns on until the thermostat reaches 7.22 °C. Then, a cam-driven operation rotates both the ejector blades and the shut-off arm for two full revolutions.

During the first rotation, the ejector blades dislodge the 8 fused together particles, which break apart as they impact the bucket below. The custom designed ice level sensing arm is connected via a linkage to the wire shut-off arm, which rotates up while the ice falls into the bin and then back down again on top of the ice. If the newly dispensed ice level is high enough, the level sensing arm will push up on the shut-off arm, which will actuate a switch that turns the icemaker off as shown in Figure 1b.

2.2 Bucket Dispense

The first dispenser system consists of a bucket that sits on slides where ice is "dispensed" by the user pulling out the bucket in the z direction (Figure 1b) and scooping ice from the bucket. In this system, the design of the custom level sensing arm is critical to proper ice level sensing and dispenser function. Improper design will result in ice production being shut off either too early (bucket will appear empty) or too late (ice level will be too high and cubes may fall behind the bucket when the bucket is pulled forward). In addition, the interaction of the custom arm with the bucket presents more potential issues such as binding when the bucket is pulled forward/backward or dragging ice off the back of the bucket when the bucket is pulled forward.

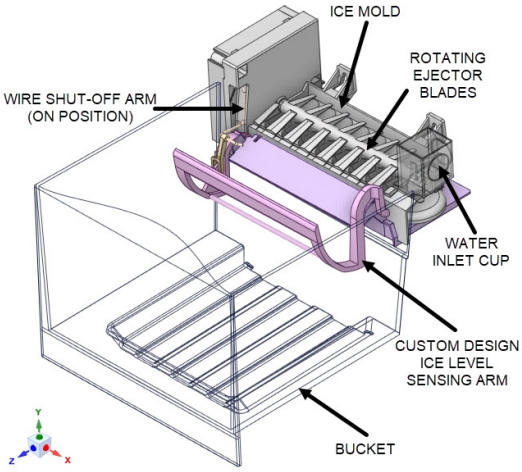

(a) Icemaker components.

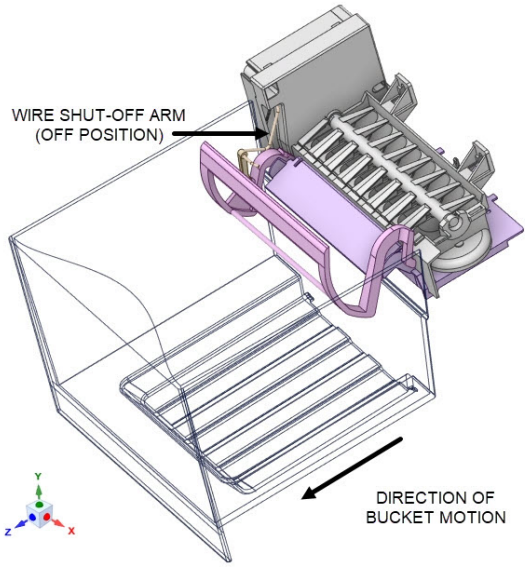

(b) Wire shut-off arm in off position.

Figure 1: Icemaker description

2.3 Auger Dispenser

The second type of dispenser system includes a secondary auger located inside the bucket that rotates to dispense the ice through a chute and into a customer's glass when the dispense button is pushed, as shown in Figure 2. Considerations with this type of design are in ensuring a consistent flow of ice through the chute (no cube jamming), determining how older ice mixes with newer ice (if a first-in-first-out design is desirable) and ensuring the forces from the falling ice exerted on the customer's glass are low enough to avoid damage to the glass or to the ice.

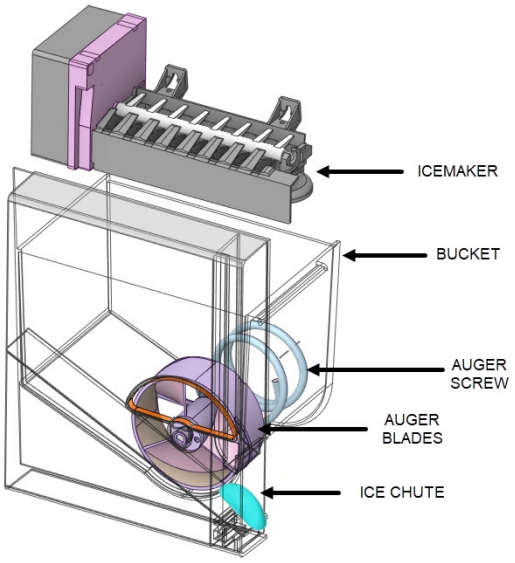

Figure 2: Auger Dispense.

3. DEM MODELING APPROACH

3.1 Governing Equations

The ice particles are modeled in the Rocky DEM software (ESSS Rocky, 2022) using the Discrete Element Method approach (DEM), a numerical technique for predicting the behavior of bulk solids. In the frame of the DEM, all particles within the computational domain are tracked in a Lagrangian way, by solving the laws that govern translational and rotational particle motion, respectively:

$$m_p \frac{d\mathbf{v}_p}{dt} = \mathbf{F}_c + m_p \mathbf{g} \tag{1}$$

$$\mathbf{J}_p \frac{d\boldsymbol{\omega}_p}{dt} = \mathbf{M}_c \tag{2}$$

where m_p is the particle mass, $\mathbf{v}_p$ is the particle velocity, $\mathbf{g}$ is the gravitational acceleration, $\boldsymbol{\omega}_p$ is the particle angular velocity, $\mathbf{F}_c$ is the contact force that accounts for particle-particle and particle-wall interactions, $\mathbf{J}_p$ is the particle moment of inertia tensor and $\mathbf{M}_c$ is the net torque generated by tangential forces that causes the rotation of the particle.

The hysteretic linear spring model (Walton & Braun, 1986) is used to compute the normal contact force. This elastic-plastic (repulsive and dissipative) model is described by the following set of equations:

$$F_n^t = \begin{cases} \min\left(K_{nl}\, s_n^t,\ F_n^{t-\Delta t} + K_{nu}\, \Delta s_n\right) & \text{if } \Delta s_n \geqslant 0 \\ \max\left(F_n^{t-\Delta t} + K_{nu}\, \Delta s_n,\ \lambda\, K_{nl}\, s_n^t\right) & \text{if } \Delta s_n < 0 \end{cases} \tag{3}$$

where F_n^t and $F_n^{t-\Delta t}$ are the normal elastic-plastic contact forces at the current time t and at the previous time $t - \Delta t$, respectively, where Δt is the timestep; K_{nl} and K_{nu} are the values of loading and unloading contact stiffnesses, respectively; $\lambda = 0.001$ is a dimensionless small constant and Δs_n is the change in the contact normal overlap during the current time, assumed to be positive as particles approach each other and negative when they separate.

The loading and unloading equivalent stiffnesses are defined, respectively, as:

$$\frac{1}{K_{nl}} = \begin{cases} \frac{1}{K_{nl,p_1}} + \frac{1}{K_{nl,p_2}} & \text{for particle-particle contact} \\ \frac{1}{K_{nl,p}} + \frac{1}{K_{nl,b}} & \text{for particle-boundary contact} \end{cases} \tag{4}$$

$$K_{nu} = \frac{K_{nl}}{\varepsilon^2} \tag{5}$$

where subscripts 1 and 2 identify the two contacting particles. The individual stiffnesses associated to a particle and to a boundary are computed, respectively, as:

$$K_{nl,p} = E_p\, L \tag{6}$$

$$K_{nl,b} = E_b\, L \tag{7}$$

where E_p is the particle material's bulk Young's modulus, E_b is the boundary material's Young's modulus, and L is the particle size.

For the tangential force calculation, an elastic-frictional model was used with the restriction that the tangential force computed by a purely elastic model cannot exceed the Coulomb's limit, as shown in Equation 8:

$$\mathbf{F}_\tau^t = \min\left(|\,\mathbf{F}_{\tau,e}^t\,|,\ \mu F_n^t \right) \frac{\mathbf{F}_{\tau,e}^t}{|\,\mathbf{F}_{\tau,e}^t\,|} \tag{8}$$

where F_n^t is the contact normal force at time t and μ is the friction coefficient. The purely elastic tangential force $\mathbf{F}_{\tau,e}^t$ is given by:

$$\mathbf{F}_{\tau,e}^t = \mathbf{F}_\tau^{t-\Delta t} - K_\tau\, \Delta \mathbf{s}_\tau \tag{9}$$

where $\mathbf{F}_\tau^{t-\Delta t}$ is the value of the tangential force at the previous time, $\Delta \mathbf{s}_\tau$ is the tangential relative displacement of the particles during the timestep and K_τ is the tangential stiffness, defined here as equal to the loading normal stiffness, $K_\tau = K_{nl}$.

3.2 Contact Detection

In this study, the actual particle shape was considered with all its geometrical features preserved. However, the accuracy increase due to the usage of custom polyhedrons including sharp edges comes with the drawback of increasing the contact detection complexity when compared with traditional spherical particles, for which checking the centroid positions and comparing them with the particle diameter would suffice.

Figure 3a illustrates the contact detection procedure for custom particle shapes. As soon as particles approach one another, it is necessary to check whether any contact is taking place. In order to do that, the distance has to be measured from the surface of the particles instead of their centroids. To reduce the computational burden, a bounding box wraps up each particle and the distance between bounding boxes is computed. When bounding boxes start to overlay, the actual distance has to be computed to check for possible contacts. During this step, a complex loop is performed to distinguish between vertex-to-vertex, vertex-to-edge, vertex-to-face, edge-to-edge, edge-to-face, or even face-to-face contact types. As illustrated in figure 3b, when a contact plane is defined, the magnitude of the overlap, meaning by how much particles penetrate each other, is used to compute contact forces.

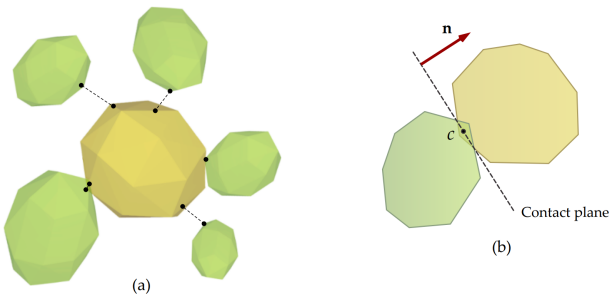

Figure 3: Contact detection

3.3 Ice Particle Modeling and Calibration

The custom polyhedron, concave particle shape shown in Figure 4b was used for all simulations. A fine mesh (1271 facets) was used in order to ensure the accurate capture of multiple particle-particle and particle-boundary interactions, as discussed in Section 3.2. All ice particles were modeled as single particles despite being connected by a small ice

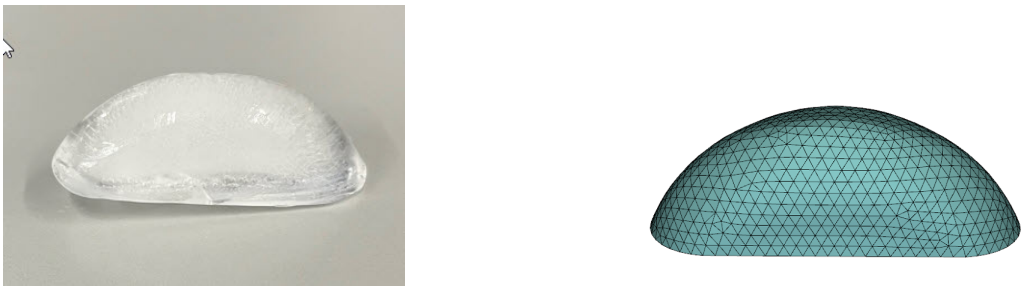

(a) Experiment **(b)** Simulation

Figure 4: Ice particle – (a) Actual ice particle, (b) Simulation particle - 1271 facets.

bridge in the mold. A more computationally expensive bonding and breakage model was not used since the ice particles generally break apart into individual cubes during harvest or upon impact with the container.

In order to predict realistic build-up of ice underneath the icemaker it was necessary to first calibrate the DEM parameters to be used for the particles interaction calculations. A drained angle of repose test was conducted by building a rectangular box ($23.5 \times 5.5 \times 12.4\,\text{in}^3$) with 5.75 in trap door in the center. The box was filled with ice (880 particles) and the trap door was removed allowing ice to drain out, as shown in Figure 5a. The experiment was repeated 7 times, with the average angle of repose on both sides being 10 deg.

The drained angle of repose setup was then reproduced in the simulation with the same dimensions and number of particles, as shown in Figure 5b. The friction factors for particle-particle and particle-boundary interactions were modified until the angle of repose results matched the experimental value. Both static and dynamic friction factors for particle-particle interaction were set to 0.1 and both particle-boundary static and dynamic friction factors were set to 0.3. Table 1 lists the final set of DEM parameters used in the simulations.

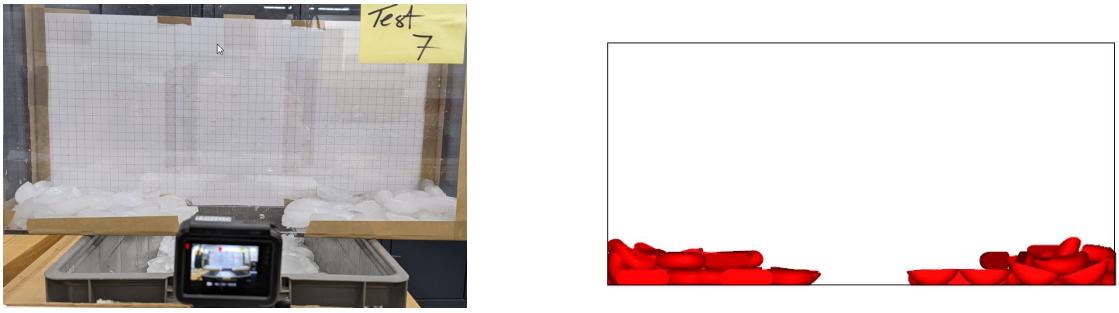

(a) **(b)**

Figure 5: Drained angle of repose – Comparison between (a) experimental and (b) numerical results.

Table 1: Particle parameters.

Property	**Value**
Size (L x W x H)	$2.4 \times 0.81 \times 0.54\,\text{in}^3$
Density	$916.7\,\text{kg m}^{-3}$
Young's modulus	0.01 GPa
Poisson's ratio	0.33
Restitution coefficient	0.3
Particle-particle friction coefficient	0.1
Particle-boundary friction coefficient	0.2

4. RESULTS

4.1 Bucket Dispensing

In the bucket dispense simulation, ice particles were set up to be injected into the mold every 2 seconds and the ejector blades were set to make a full rotation every 2 seconds to harvest particles from the icemaker and into the bucket. Figure 6 shows the position of the ice level sensing arm and ejector blades during one full cycle. At the beginning of the cycle, the sensing arm was at rest on top of the cubes in the bucket. It was then set to rotate 45° while the ejector blades pushed the ice into the bucket. Next, a free body rotation was applied to the sensing arm so that the arm rotated down to rest on top of the newly harvested ice. This process was repeated until the ice sensing arm reached the 25° shut off angle due to the build up of ice underneath it. Next, a translational velocity of 0.228 69 m s^{-1} was assigned to the bucket to move it out from under the arm in order to determine if ice would fall off of the back of the bucket.

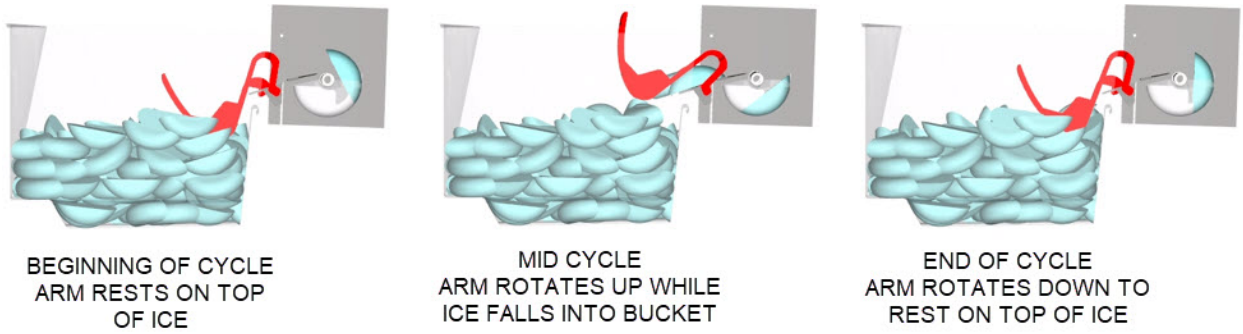

Figure 6: Ice Harvest Process.

Customers perceive ice falling outside the bucket as a nuisance and as a sign that the design is not operating as intended. As shown in Figure 7, the simulation was able to replicate a particle of ice (circled in red in the experimental test (Figure 7a) and colored in red in the simulation (Figure 7b)) falling off the back of the bucket due to the way that the ice builds up above the sensing arm. This calibrated DEM model allows for the quick simulation of multiple design iterations, in order to develop a solution that eliminates this issue.

A future step in this analysis would be to couple the DEM software with a multi-body dynamics software to ensure the new sensing arm will not bind with the bucket and to predict potential issues with wear over time.

(a) **(b)**

Figure 7: Ice falling off the bucket – Comparison between (a) experimental and (b) numerical results.

4.2 Auger Dispensing

The purpose of the first auger dispense simulation was to determine if the DEM model was able to reproduce the dispensing behavior of the existing design. Therefore, a half-full bucket was chosen to simplify the experimental tests, in which 10 batches of ice were harvested from the icemaker and into the bucket using the same cyclic injection of ice

as was used in the bucket dispensing simulation (see section 4.1). Next, a rotational velocity of $4\,\mathrm{rad\,s^{-1}}$ was assigned to the auger mechanism to dispense the ice into a container.

In order to evaluate the mixing of new and old ice cubes through the auger mechanism, each batch of ice was colored differently, allowing the residence time and mixing to be evaluated experimentally, as shown in Figure 8a. The same was reproduced numerically, as shown in Figure 8b, with particles colored by their residence time inside the bucket.

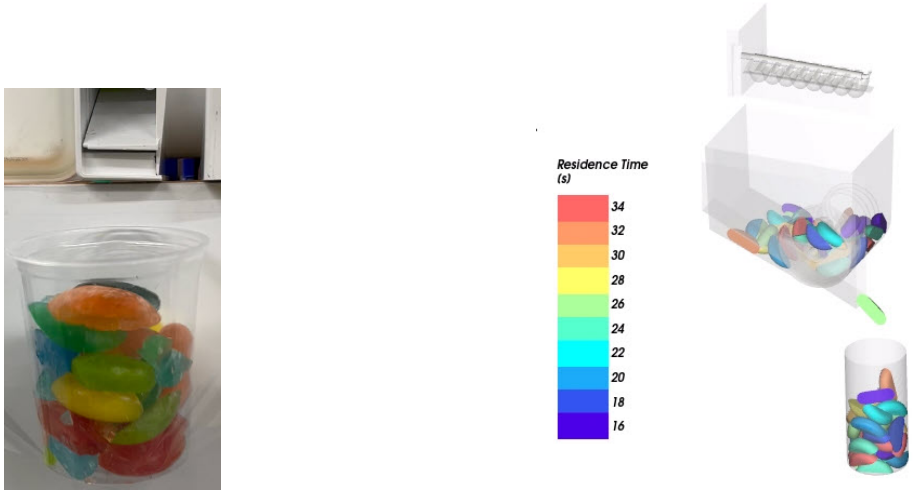

(a) **(b)**

Figure 8: Residence time comparison between (a) experimental and (b) numerical results.

Using the coloring strategy with a known dispensing cycle, the residence time of the ice cubes inside the buckets can be calculated for each particle in the experimental tests. Figure 9 shows the comparison of the residence time distribution of the ice cubes dispensed into the container obtained in the experimental tests and in the numerical simulation, showing that due to the design of the auger mechanism and bucket, older and newer ice mix relatively evenly when the bucket is only half full.

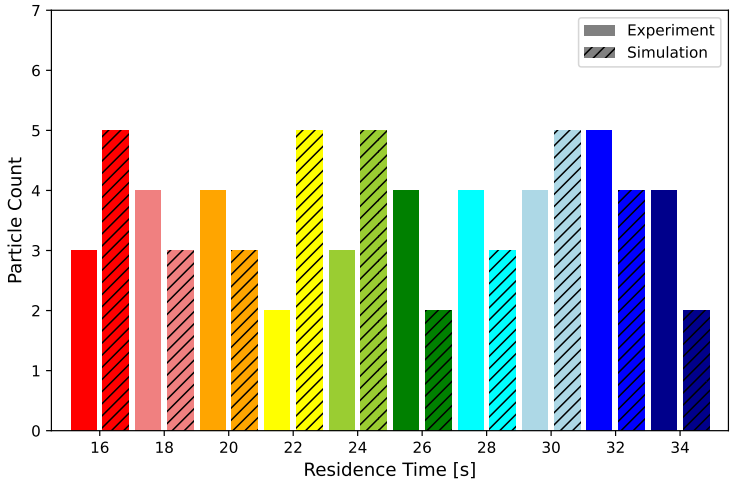

Figure 9: Comparison of the residence time distribution of the ice cubes dispensed into the container obtained in the experimental test and in the numerical simulation

In order to investigate the influence of the ice position on the dispensing order in normal operation, in which the icemaker produces ice until the bucket is full, a second version of this simulation was performed using twice the quantity of cubes dispensed into the bucket. As shown in Figure 10a, ice cubes were tagged by their horizontal position inside the bucket before the dispenser process started. Figure 10b shows the ice particles at 23.5 s, after half of the ice has been dispensed, and clearly indicates that dark blue ice cubes on the far left side of the bucket will be the last to be dispensed. Figure 10c shows the distribution of ice dispensed into the container after 23.5 seconds based on initial location. The column of ice second from the right (shown in yellow) represents a significant majority of the cubes, followed by ice in the far right column (shown in red). Ice to the left of the auger blades was much less represented. This information can inform how to improve auger and bucket design if a first-in-first-out dispensing design is desired.

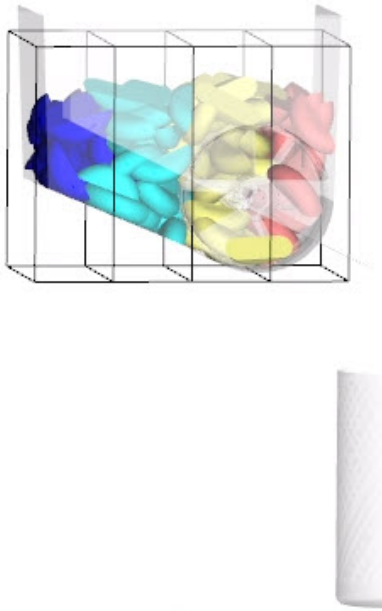

(a) Position based tagging prior to dispense

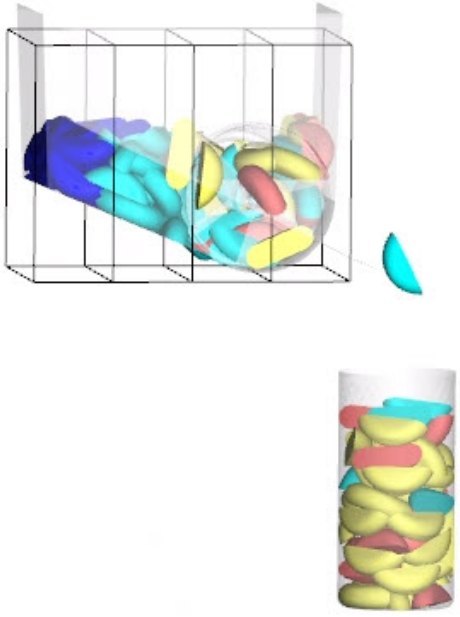

(b) Tagging after half of the ice is dispensed

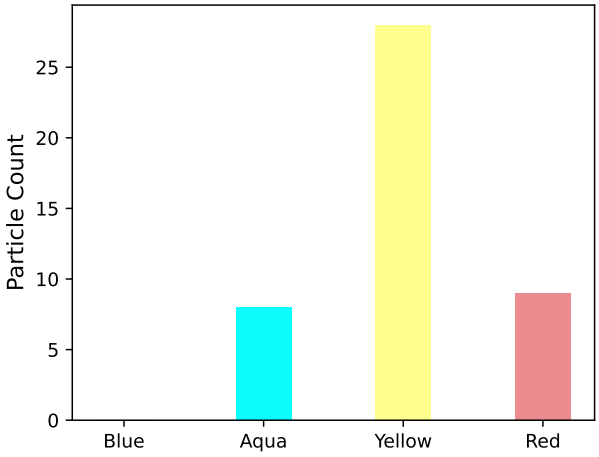

(c) Particle tagging distribution in the container after half of the ice is dispensed

Figure 10: Dispensing order evaluation (a) tagging particles based on their position at the bucket before the process starts (b) after half of the ice is dispensed (c) particle tagging distribution in the container.

The DEM model also allows for the evaluation of the impact forces on the bucket and container as well as the com-

pression forces exerted by the auger on the ice to understand if damage to the ice would occur. To validate the impact force exerted on the bottom of the container from the falling ice, a Dytran Model 3055D1 accelerometer was affixed to a metal container, which was clamped to a table at the same distance from the dispenser outlet as the container in the simulation, as shown in Figure 11a. Acceleration data was collected and multiplied by the average cube mass of 13.7 g. As shown in the Figure 11b, the resulting experimental data was within the same order of magnitude as the simulation data, which also used a ice mass of 13.7 g. This data can be used to ensure that the dispenser design keeps forces low enough so that there is no breakage or damage to the ice or the container.

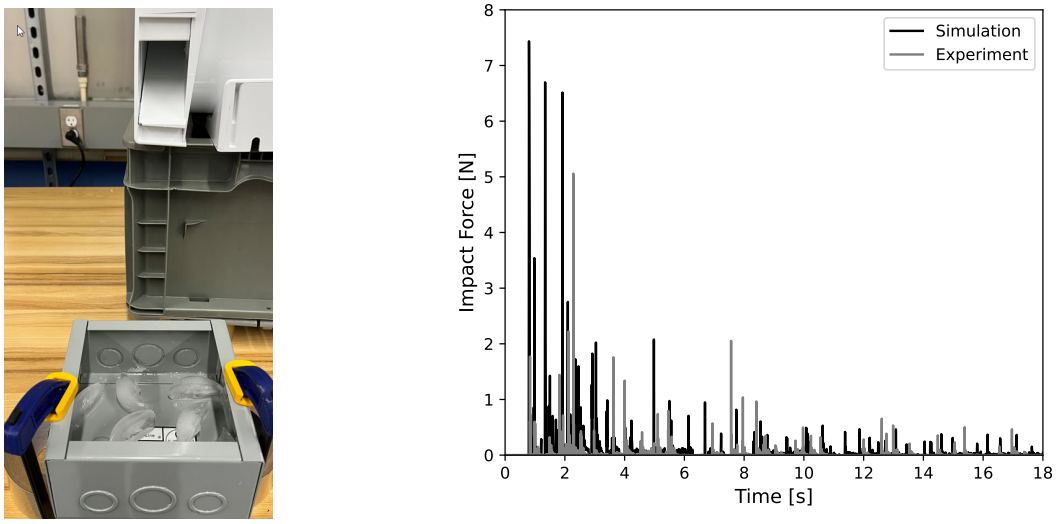

(a) **(b)**

Figure 11: (a) Accelerometer experimental set up. (b) Comparison between experimental and numerical impact force results.

Compression forces from the auger pushing the ice against the bottom of the dispenser bucket were also studied. An experiment using a Tinius Olsen H50K tensile tester was performed to investigate the compression force limits for an ice particle. For this test, an ice cube was placed on an aluminum block with a paper towel under it to prevent sliding. The tensile tester was set up for constant displacement (50.8 mm/min). The results obtained for 7 samples are summarized in Table2.

Table 2: Tinius Olsen H50K Compression force testing (n = 7).

	Breaking Force (N)
Min	898.5
Max	1227.7
Average	1044.0

To investigate if ice particles are prone to any damage as they interact with the dispensing auger, the maximum normal force was collected in the DEM simulation during 18 s, or about 11.5 auger revolutions. Figure 12 compares the maximum normal force on particles obtained during the simulation with the minimum, maximum, and average experimental forces, shown by horizontal lines. It can be seen that as long as the auger is able to maintain rotation, there is a chance that damage could occur to some of the ice cubes due to the excessive compression force of the auger. Moreover, it is possible that similar scenarios could also damage the auger or contribute to lower its lifespan if improper materials are chosen for its components. The DEM model can be used to evaluate different auger designs and operational processes that can mitigate ice and auger damages.

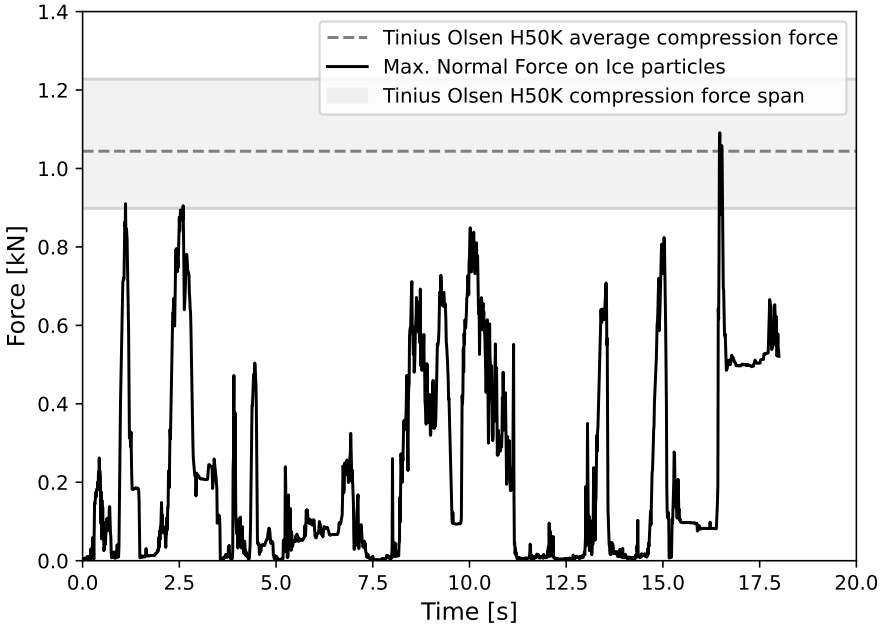

Figure 12: Maximum normal force experienced by the particles during ice dispensing

5. CONCLUSIONS

The validated DEM model for the bucket dispense system can be used to evaluate multiple ice sensing arm and bucket designs to ensure that the ice level is sensed properly and that the arm does not drag any ice particles off the back of the bucket. The validated DEM model for the auger dispensing system demonstrates that the mixing of ice in the bucket based on residence time is highly dependent on the level of ice and position of the cubes inside the bucket. This information can be used to inform auger and bucket design to ensure the oldest ice is dispensed first. In addition, the compression and impact forces for particles and components captured in the collision statistics can be used to inform the design to mitigate damage to both ice and component parts. DEM simulations can be performed to evaluate improvements for both types of dispenser designs to avoid common design issues and to reduce prototype cycle time and costs.

REFERENCES

ESSS Rocky. (2022). DEM Technical Manual, Release 2022 R1 [Computer software manual].

Fernandez, J. W., Cleary, P. W., Mcbride, W., et al. (2009). Effect of screw design on hopper draw down by a horizontal screw feeder. In *Seventh international conference on cfd in the minerals and process industries csiro, melbourne, australia* (pp. 9–11).

Sun, H., Ma, H., & Zhao, Y. (2022). Dem investigation on conveying of non-spherical particles in a screw conveyor. *Particuology*, *65*, 17-31.

Walton, O. R., & Braun, R. L. (1986). Viscosity, granular-temperature, and stress calculations for shearing assemblies of inelastic, frictional disks. *Journal of Rheology*, *30*, 948–980.

ACKNOWLEDGMENT

The authors thank Jason Konz, Nathan Lindgren and Ben Trihey at Sub-Zero Group, Inc. for assistance with experimental test set-up and data acquisition.